Photoproduction of P-wave doubly charmed baryon at future e^+e^- collider

Xi-Jie Zhan,[a,b,1] **Xing-Gang Wu**[a,b] **and Xu-Chang Zheng**[a,b]

[a]*Department of Physics, Chongqing University,*
Chongqing 401331, People's Republic of China

[b]*Chongqing Key Laboratory for Strongly Coupled Physics, Chongqing University,*
Chongqing 401331, People's Republic of China

E-mail: zhanxj@cqu.edu.cn, wuxg@cqu.edu.cn, zhengxc@cqu.edu.cn

ABSTRACT: The photoproduction of P-wave doubly charmed baryon (Ξ_{cc}) is investigated in the context of future high-energy and high-luminosity e^+e^- colliders. The direct photoproduction via the sub-process $\gamma+\gamma \to \Xi_{cc}+\bar{c}+\bar{c}$ and the resolved channel $\gamma+g \to \Xi_{cc}+\bar{c}+\bar{c}$ are considered. Within the framework of non-relativistic QCD, the calculation encompasses four P-wave (cc)-diquark configurations: $(cc)_{\bar{3}}[^1P_1]$, $(cc)_{6}[^3P_0]$, $(cc)_{6}[^3P_1]$ and $(cc)_{6}[^3P_2]$. The two S-wave states, $(cc)_{\bar{3}}[^3S_1]$ and $(cc)_{6}[^1S_0]$, are also included for comparison. The cross sections, as well as the differential distributions involving transverse momentum, rapidity, and angular variables, have been computed. Numerical results reveal that the resolved photoproduction process plays a significant role and can provide dominant contributions. The photoproduction rate of the P-wave Ξ_{cc} is approximately one order of magnitude lower than that of the S-wave.

---

[1]Corresponding author.

Contents

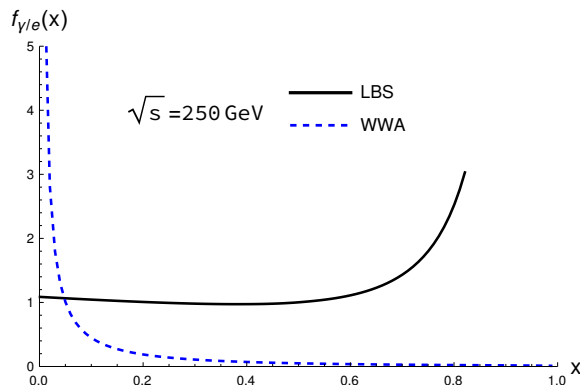## 1 Introduction

A doubly heavy baryon is a system composed of two heavy quarks and one light quark. It possesses a simple structure akin to that of a heavy quarkonium, which enables rigorous theoretical analysis. As a result, investigating its production properties is believed to aid in understanding and validating the theory of Quantum Chromodynamics (QCD). In 2002 and 2005, the SELEX Collaboration reported a possible discovery of the Ξ_{cc}^+ baryon [1, 2]. More recently, in 2017, the LHCb Collaboration confirmed the existence of another type of doubly heavy baryon, Ξ_{cc}^{++}, through the decay channel $\Xi_{cc}^{++} \to \Lambda_c^+ K^- \pi^+ \pi^+$ ($\Lambda_c^+ \to pK^-\pi^+$). The measured properties of mass and lifetime for this Ξ_{cc}^{++} baryon were found to be in excellent agreement with theoretical calculations. Subsequently, the LHCb Collaboration further confirmed its existence in the decay $\Xi_{cc}^{++} \to \pi^+\Xi_c^+$ [3, 4]. The genuine discovery of doubly heavy baryons is poised to trigger a new wave of theoretical research.

Due to the inherent nonrelativistic characteristics coupled with the confinements attributed to strong interactions, the production of doubly heavy baryons encompasses intricate nonperturbative effects that elude computation through conventional perturbative QCD methods. The study conducted by Ma et al. [5] undertook the task of describing this production process through the utilization of the nonrelativistic QCD (NRQCD) factorization framework [6]. This ingenious framework dissects the procedure into two sequential stages: firstly, the perturbative formation of a heavy-quark pair within a distinct quantum state, often referred to as a diquark, followed by its subsequent nonperturbative transformation into a baryon. By employing an expansion rooted in the heavy quark's diminished velocity (v_Q) within the rest frame of the baryon, the study was able to pinpoint two foremost states of (cc)-diquarks at the leading order: $_{\bar{3}}[^3S_1]$ and $_{6}[^1S_0]$. These diquark states respectively correspond to the $^3S_1$ and $^1S_0$ S-wave configurations, while existing in the $\bar{\mathbf{3}}$ and $\mathbf{6}$ color states. Accompanying these states are the associated long-distance matrix elements (LDMEs), denoted as $h_{\bar{\mathbf{3}}}$ and $h_{\mathbf{6}}$, which encapsulate the nonperturbative likelihood of their transition into the baryonic state.

Numerous comprehensive theoretical investigations have delved into the realm of producing doubly heavy baryons [7–37]. These investigations have encompassed a range of

Figure 1. The energy spectra of the LBS photon and the WWA photon.

production mechanisms, including direct processes occurring in *pp*, *ep*, $\gamma\gamma$, and e^+e^- collisions, as well as indirect channels involving the decays of Higgs bosons, W and Z bosons, and top quarks. For the purpose of simulating hadroproduction in *pp* collisions, a dedicated generator known as GENXICC [38–40] has been meticulously developed.

Next-generation e^+e^- colliders have been put forth in recent times, among them being the FCC-ee [41], the CEPC [42, 43], and the ILC [44, 45]. These cutting-edge colliders are designed to operate at high collision energies and are projected to achieve unparalleled luminosities. As a result of their capabilities, these advanced e^+e^- colliders hold immense potential to serve as exceptional platforms for a wide array of research topics. The e^+e^- collider provides two main pathways for the direct production of the doubly heavy baryon Ξ_{cc}: production through e^+e^- annihilation and via the photoproduction mechanism. In this work, Ξ_{cc} denotes the baryon Ξ_{ccq}, where q corresponds to an up (u), down (d), or strange (s) quark. Regarding photoproduction, the Ξ_{cc} baryon can be generated through direct photon-photon fusion, such as $\gamma + \gamma \to \Xi_{cc} + \bar{c} + \bar{c}$. Beyond direct photoproduction, another category of processes, known as resolved photoproduction [46], exists. In these cases, the photon undergoes a process of resolution, leading to its parton's involvement in the subsequent hard processes. The resolved photoproduction channels share a comparable order of perturbative expansion with the direct approach, underscoring the need for their incorporation in calculations. Earlier investigations [46–51] have indicated that the single resolved channel($\gamma + g$) tend to exert a dominant influence on the photoproduction of heavy quarkonium and doubly heavy baryon at e^+e^- colliders. The contributions stemming from double resolved photoproduction channels are generally negligible and can be safely ignored.

In this work, we offer an analysis of the photoproduction of *P*-wave doubly charmed baryon at future e^+e^- collider. Based on the NRQCD factorization framework, we will consider two types of photoproduction processes: $\gamma + \gamma \to \Xi_{cc} + \bar{c} + \bar{c}$ and $\gamma + g \to \Xi_{cc} + \bar{c} + \bar{c}$. For (cc)-diquark, the quantum number is $(cc)_{\bar{\mathbf{3}}}[^3S_1]$, $(cc)_{\mathbf{6}}[^1S_0]$, $(cc)_{\bar{\mathbf{3}}}[^1P_1]$ or $(cc)_{\mathbf{6}}[^3P_J]$ with $J = 0, 1, 2$. Section 2 provides the formulation of the calculation, while section 3 presents the numerical results and subsequent discussions. Section 4 gives a brief summary.

2 Formulation and calculation

In the photoproduction process at the e^+e^- collider, the colliding photon can originate either from the bremsstrahlung of the initial e^+e^- particles or from the process of laser back-scattering with e^+e^- [44]. The energy spectrum of the bremsstrahlung photon can be characterized using the Weizäcker-Williams approximation (WWA) [52], whereas the spectrum originating from laser back-scattering (LBS) is parameterized in ref. [53]. The two spectra exhibit distinct behaviors, as illustrated in figure 1. It is observed the laser back-scattering (LBS) mechanism generates a greater number of high-energy photons, potentially resulting in a significantly higher photoproduction rate compared to the WWA photons. For the sake of simplicity, in this study, our calculations and analysis are primarily based on the use of LBS photons. The spectrum is as follows:

$$f_{\gamma/e}(x) = \frac{1}{N}\left[1 - x + \frac{1}{1-x} - 4r(1-r)\right], \tag{2.1}$$

where $x = E_\gamma/E_e$, $r = x/(x_m(1-x))$, and the normalization factor is given by:

$$N = \left(1 - \frac{4}{x_m} - \frac{8}{x_m^2}\right)\log(1 + x_m) + \frac{1}{2} + \frac{8}{x_m} - \frac{1}{2(1+x_m)^2}. \tag{2.2}$$

Here, $x_m = 4E_eE_l\cos^2\frac{\theta}{2}$, with E_e and E_l representing the energies of the incident electron and laser beams, respectively, and θ denoting the angle between them. The range of energy for the laser back-scattering (LBS) photon is constrained by:

$$0 \le x \le \frac{x_m}{1 + x_m}, \tag{2.3}$$

with the optimal value of x_m being 4.83 [54].

As mentioned earlier, our calculations will rely on the NRQCD factorization framework, which has achieved significant success in describing heavy quarkonia production. While an all-order proof of NRQCD factorization for quarkonium production is currently lacking, it has been observed that this factorization holds up to at least the next-to-next-to-leading order (NNLO) in α_s when the LDMEs are adjusted to achieve gauge completeness [55–57]. In this work, our leading order calculation for Ξ_{cc} photoproduction are free of infrared singularities. Within the framework of NRQCD, the photoproduction cross-section of Ξ_{cc} at the e^+e^- collider can be represented as follows:

$$\begin{aligned}
d\sigma(e^+e^- \to e^+e^-\Xi_c + \bar{c} + \bar{c}) = &\int dx_1 f_{\gamma/e}(x_1) \int dx_2 f_{\gamma/e}(x_2) \\
&\times \sum_{i,j} \int dx_i f_{i/\gamma}(x_i) \int dx_j f_{j/\gamma}(x_j) \\
&\times \sum_n d\hat{\sigma}(ij \to (cc)[n] + \bar{c} + \bar{c})\left\langle\mathcal{O}^{\Xi_{cc}}[n]\right\rangle. \tag{2.4}
\end{aligned}$$

Here, $f_{\gamma/e}(x)$ represents the energy spectrum of the photon. $f_{i/\gamma}$ ($i = \gamma, g, u, d, s$) corresponds to the Glück-Reya-Schienbein (GRS) distribution function of parton i within the photon [58]. $f_{\gamma/\gamma}(x) = \delta(1-x)$ is utilized for the direct photoproduction process.
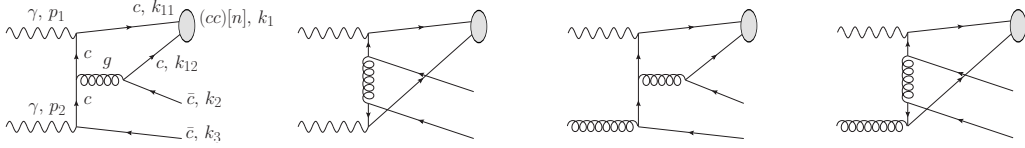
Figure 2. Some Feynman diagrams of the partonic processes for Ξ_{cc} photoproduction. The diagrams are drawn by JaxoDraw [63].

$d\hat{\sigma}(ij \to (cc)[n] + \bar{c} + \bar{c})$ denotes the differential partonic cross-section, which is evaluated perturbatively. For the baryons Ξ_{cc}, $(cc)[n] = (cc)_{\bar{3}}[^3S_1]$, $(cc)_{6}[^1S_0]$, $(cc)_{\bar{3}}[^1P_1]$ or $(cc)_{6}[^3P_J]$. $\langle \mathcal{O}^{\Xi_{cc}}[n] \rangle = h_{\bar{3}(6)}$ denotes the long-distance matrix element (LDME). Typically, people adopt a potential model approach, drawing parallels with the heavy quarkonium scenario, and introduce and correlate a wave function with $h_{\bar{3}}$ [7, 59–62],

$$h_{\bar{3}} \simeq |\Psi_{cc}(0)|^2 \, \text{or} \, |\Psi'_{cc}(0)|^2. \tag{2.5}$$

Regarding h_{6}, there exists no specific relation, and for the sake of simplicity, it is assumed to be equal to $h_{\bar{3}}$. This assumption is rooted in NRQCD's power counting relative to v_c, where both h_{6} and $h_{\bar{3}}$ are assigned equivalent orders [5]. In accordance with NRQCD, the bound state Ξ_{cc} can be expanded into a series of Fock states:

$$|\Xi_{cc}\rangle = c_1(v)|(cc)q\rangle + c_2(v)|(cc)qg\rangle + c_3(v)|(cc)qgg\rangle + \cdots. \tag{2.6}$$

Because a light quark can easily emit gluons, the constituents in eq. (2.6) carry equivalent significance, specifically, $c_1 \sim c_2 \sim c_3$. Consider a cc pair in the $\bar{3}[^3S_1]$ state; one of the heavy quarks can emit a gluon without altering the spin of the heavy quark. Subsequently, this emitted gluon can undergo a splitting process, leading to the formation of a light quark-antiquark pair $q\bar{q}$. This allows the heavy cc pair to interact with the light q and form the composite particle Ξ_{cc}. Similarly, for a cc pair in the $6[^1S_0]$ state, one of the heavy quarks can emit a gluon while preserving the spin of the heavy quark. This emitted gluon then separates into a light $q\bar{q}$ pair, and the light quarks also have the capability to emit gluons. Consequently, this heavy cc pair can capture a light quark and a gluon to assemble into Ξ_{QQ}. This is the reason for h_{6} and $h_{\bar{3}}$ holding the same order in v_c. For the sake of simplicity, we assume $h_{6} = h_{\bar{3}}$ in the subsequent calculations. It is worth noting that the long-distance matrix elements (LDMEs) function as overarching parameters beyond the perturbative components, indicating that the results can be refined with the acquisition of new LDMEs.

For the partonic processes in leading order of α_s, there are 40 Feynman diagrams for $\gamma + \gamma \to \Xi_{cc} + \bar{c} + \bar{c}$ and 48 diagrams for $\gamma + g \to \Xi_{cc} + \bar{c} + \bar{c}$, as exemplified in figure 2. In practical calculations, we apply charge conjugation $C = -i\gamma^2\gamma^0$ to reverse the one of the $c \sim \bar{c}$ fermion chains, such as $L_1 = \bar{u}_{s_1}(k_{12})\Gamma_{i+1}S_F(q_i, m_i)\cdots S_F(q_1, m_1)\Gamma_1 v_{s_2}(k_2)$. Here, Γ_i represents the interaction vertex, $S_F(q_i, m_i)$ denotes the fermion propagator, where q_i and m_i are the respective momentum and mass parameters. The subscripts s_1 and s_2 are used for spin indices, while the index i enumerates the fermion propagators ($i = 0, 1, \ldots$)

along this fermion line. The conversion obeys:

$$
\begin{aligned}
v_{s_2}^T(k_2)C &= -\bar{u}_{s_2}(k_2), \\
C^- \bar{u}_{s_1}(k_{12})^T &= v_{s_1}(k_{12}), \\
C^- S_F^T(-q_i, m_i)C &= S_F(q_i, m_i), \\
C^- \Gamma_i^T C &= -\Gamma_i.
\end{aligned}
\tag{2.7}
$$

L_1 is reversed to:

$$
\begin{aligned}
L_1 = L_1^T &= v_{s_2}^T(k_2)\Gamma_1^T F_F^T(q_1, m_1)\cdots S_F^T(q_i, m_i)\Gamma_{i+1}^T \bar{u}_{s_1}^T(k_{12}) \\
&= v_{s_2}^T(k_2)CC^- \Gamma_1^T CC^- S_F^T(q_1, m_1)CC^- \cdots CC^- S_F^T(q_i, m_i)CC^- \Gamma_{i+1}^T CC^- \bar{u}_{s_1}^T(k_{12}) \\
&= (-1)^{(n+1)}\bar{u}_{s_2}(k_2)\Gamma_1 S_F(-q_1, m_1)\cdots S_F(-q_i, m_i)\Gamma_{i+1}v_{s_1}(k_{12}),
\end{aligned}
\tag{2.8}
$$

here n is the number of vector vertices in the fermion chain. Let us take the first diagram in figure 2 as an example, its amplitudes read:

$$
\begin{aligned}
M_1 \sim \frac{1}{(k_{12} + k_2)^2}&\bar{u}_{s12}(k_{12})\gamma^\mu v_{s2}(k_2)\bar{u}_{s11}(k_{11}) \not{\epsilon}(p_1) \\
&\times \frac{\not{p}_2 - \not{k}_{12} - \not{k}_2 - \not{k}_3 + m_c}{(\not{p}_2 - \not{k}_{12} - \not{k}_2 - \not{k}_3)^2 - m_c^2}\gamma_\mu \frac{\not{p}_2 - \not{k}_3 + m_c}{(\not{p}_2 - \not{k}_3)^2 - m_c^2} \not{\epsilon}(p_2)v_{s3}(k_3),
\end{aligned}
\tag{2.9}
$$

Where k_{11} and k_{12} are momenta of the two c quarks. In the diquark state, their relative momentum q is small and we can set $k_{11} = \frac{m_c}{M_{cc}}k_1 + q$ and $k_{12} = \frac{m_c}{M_{cc}}k_1 - q$ with k_1 being the momentum of the diquark. Here the diquark mass $M_{cc} = 2m_c$ is adopted in order to ensure the gauge invariance of the amplitude. After reverse the first fermion line, the amplitude becomes:

$$
\begin{aligned}
M_1 \sim -\frac{1}{(k_{12} + k_2)^2}&\bar{u}_{s2}(k_2)\gamma^\mu v_{s12}(k_{12})\bar{u}_{s11}(k_{11}) \not{\epsilon}(p_1) \\
&\times \frac{\not{p}_2 - \not{k}_{12} - \not{k}_2 - \not{k}_3 + m_c}{(\not{p}_2 - \not{k}_{12} - \not{k}_2 - \not{k}_3)^2 - m_c^2}\gamma_\mu \frac{\not{p}_2 - \not{k}_3 + m_c}{(\not{p}_2 - \not{k}_3)^2 - m_c^2} \not{\epsilon}(p_2)v_{s3}(k_3).
\end{aligned}
\tag{2.10}
$$

Now we can replace $v_{s12}(k_{12})\bar{u}_{s11}(k_{11})$ by the spin projector for $(c\bar{c})[n]$ to get the amplitude of $\gamma + \gamma \to (cc)[n] + \bar{c} + \bar{c}$. The spin projector takes the form of

$$
\Pi_{k_1}(q) = \frac{-\sqrt{M_{cc}}}{4m_c^2}(\not{k}_{12} - m_c)\gamma^5(\not{k}_{11} + m_c),
\tag{2.11}
$$

$$
\Pi_{k_1}^\beta(q) = \frac{-\sqrt{M_{cc}}}{4m_c^2}(\not{k}_{12} - m_c)\gamma^\beta(\not{k}_{11} + m_c),
\tag{2.12}
$$

for $n = {}^1S_0$ and ${}^3S_1$ respectively. The amplitudes of the P-wave production can be obtained

via the derivation of the S-wave expression, i.e.,

$$M_1[^1P_1] \sim \varepsilon_\alpha^l(k_1) \frac{d}{dq_\alpha} \Bigg[-\frac{1}{(k_{12}+k_2)^2} \bar{u}_{s2}(k_2)\gamma^\mu \frac{-\sqrt{M_{cc}}}{4m_c^2} (\slashed{k}_{12}-m_c)\gamma^5(\slashed{k}_{11}+m_c)\slashed{\varepsilon}(p_1)$$
$$\times \frac{\slashed{p}_2-\slashed{k}_{12}-\slashed{k}_2-\slashed{k}_3+m_c}{(\slashed{p}_2-\slashed{k}_{12}-\slashed{k}_2-\slashed{k}_3)^2-m_c^2}\gamma^\mu \frac{\slashed{p}_2-\slashed{k}_3+m_c}{(\slashed{p}_2-\slashed{k}_3)^2-m_c^2}\slashed{\varepsilon}(p_2)v_{s3}(k_3)\Bigg]\Big|_{q=0}, \quad (2.13)$$

$$M_1[^3P_J] \sim \varepsilon_{\alpha\beta}^J(k_1) \frac{d}{dq_\alpha} \Bigg[-\frac{1}{(k_{12}+k_2)^2} \bar{u}_{s2}(k_2)\gamma^\mu \frac{-\sqrt{M_{cc}}}{4m_c^2} (\slashed{k}_{12}-m_c)\gamma^\beta(\slashed{k}_{11}+m_c)\slashed{\varepsilon}(p_1)$$
$$\times \frac{\slashed{p}_2-\slashed{k}_{12}-\slashed{k}_2-\slashed{k}_3+m_c}{(\slashed{p}_2-\slashed{k}_{12}-\slashed{k}_2-\slashed{k}_3)^2-m_c^2}\gamma^\mu \frac{\slashed{p}_2-\slashed{k}_3+m_c}{(\slashed{p}_2-\slashed{k}_3)^2-m_c^2}\slashed{\varepsilon}(p_2)v_{s3}(k_3)\Bigg]\Big|_{q=0}, \quad (2.14)$$

Here, $\varepsilon_\beta^s(k_1)$ or $\varepsilon_\alpha^l(k_1)$ represents the polarization vector associated with the spin or orbital angular momentum of the diquark in the spin triplet S-state or spin singlet P-state. $\varepsilon_{\alpha\beta}^J(k_1)$ corresponds to the polarization tensor for the spin triplet P-wave states, where J can be 0, 1, or 2. To determine the suitable total angular momentum, we appropriately perform the polarization sum. The summation over polarization vectors is carried out as follows:

$$\sum_{r_z} \varepsilon_\alpha^r \varepsilon_{\alpha'}^{r*} = \Pi_{\alpha\alpha'} \quad (2.15)$$

The summation over polarization tensors is conducted as:

$$\varepsilon_{\alpha\beta}^0 \varepsilon_{\alpha'\beta'}^{0*} = \frac{1}{3}\Pi_{\alpha\beta}\Pi_{\alpha'\beta'} \quad (2.16)$$

$$\sum_{J_z} \varepsilon_{\alpha\beta}^1 \varepsilon_{\alpha'\beta'}^{1*} = \frac{1}{2}(\Pi_{\alpha\alpha'}\Pi_{\beta\beta'} - \Pi_{\alpha\beta'}\Pi_{\alpha'\beta}) \quad (2.17)$$

$$\sum_{J_z} \varepsilon_{\alpha\beta}^2 \varepsilon_{\alpha'\beta'}^{2*} = \frac{1}{2}(\Pi_{\alpha\alpha'}\Pi_{\beta\beta'} + \Pi_{\alpha\beta'}\Pi_{\alpha'\beta}) - \frac{1}{3}\Pi_{\alpha\beta}\Pi_{\alpha'\beta'}, \quad (2.18)$$

with the definition

$$\Pi_{\alpha\beta} = -g_{\alpha\beta} + \frac{k_{1\alpha}k_{1\beta}}{M_{cc}^2}. \quad (2.19)$$

For the processes $\gamma + \gamma \to (cc)[n] + \bar{c} + \bar{c}$, the color factor $\mathcal{C}_{ij,k}$ is universal for all the Feynman diagrams and $\mathcal{C}_{ij,k} = \mathcal{N} \times \sum_{a,m,n}(T^a)_{mi}(T^a)_{nj} \times G_{mnk}$. Here $\mathcal{N} = 1/\sqrt{2}$ is the normalization constant, i, j, m, n are color indices of four heavy quarks and k denotes the color index of the diquark. G_{mnk} corresponds to either the antisymmetric function ε_{mnk} for the color anti-triplet state, or the symmetric function f_{mnk} for the color sextuplet state, and they obey

$$\varepsilon_{mnk}\varepsilon_{m'n'k} = \delta_{mm'}\delta_{nn'} - \delta_{mn'}\delta_{nm'}, \quad (2.20)$$

$$f_{mnk}f_{m'n'k} = \delta_{mm'}\delta_{nn'} + \delta_{mn'}\delta_{nm'}. \quad (2.21)$$

The color factors of diagrams for $\gamma + g \to (cc)[n] + \bar{c} + \bar{c}$ are not the same; they need to be calculated individually.

3 Numerical results and discussions

In the calculation, we adopt the wave functions at the origin from [64] as $|\Psi(0)|^2 = 0.0218\,\mathrm{GeV}^3$ and $|\Psi'(0)|^2 = 2.48 \times 10^{-3}\,\mathrm{GeV}^5$. The quark mass is set as $m_c = M_{\Xi_{cc}}/2 = 1.8\,\mathrm{GeV}$. The fine structure constant is assigned the value $\alpha = 1/137$. Regarding the strong coupling constant, we utilize the one-loop running formulation. The renormalization scale is typically taken as the transverse mass of Ξ_{cc}, specifically $\mu = \sqrt{M_{\Xi_{cc}}^2 + p_t^2}$, where p_t denotes the transverse momentum of the particle.

Table 1 lists cross sections of different photoproduction processes, where three collision energies, $\sqrt{S} = 250, 500, 1000\mathrm{GeV}$, are adopted. From the table, it is evident that the contribution from production channel $\gamma + \gamma$ decreases as the collision energy increases, while the contribution from production channel $\gamma + g$ increases with higher energy levels. As a cumulative result, the total production cross-section increases with the growth of collision energy. At $\sqrt{S} = 250\,\mathrm{GeV}$, the contribution from the $\gamma + \gamma$ channel is comparable to that of the $\gamma + g$ channel. However, as the collision energy increases, the scenario changes. The $\gamma + g$ channel begins to dominate the photoproduction process. Specifically, at $\sqrt{S} = 500\,\mathrm{GeV}$, the $\gamma + \gamma$ channel provides 20% of the contribution, while the $\gamma + g$ channel contributes 80%; and at $\sqrt{S} = 1000\,\mathrm{GeV}$, the $\gamma + \gamma$ channel provides 6% of the contribution, while the $\gamma + g$ channel contributes 94%. Table 1 clearly emphasizes the significance of the single resolved photoproduction channel. For comparison, the cross sections via WWA photons are also provided in brackets in table 1. It shows that the total production cross-section also increases with the growth of collision energy for the case of WWA photons. The contribution from the $\gamma + \gamma$ channel is larger than that of the $\gamma + g$ channel. Table 1 indicates that their total cross sections are significantly lower than those associated with the LBS photons, accounting for only 13%, 18% and 21% of the LBS photoproduction cross sections at collision energies of $\sqrt{S} = 250\,\mathrm{GeV}$, $\sqrt{S} = 500\,\mathrm{GeV}$ and $\sqrt{S} = 1000\,\mathrm{GeV}$, respectively. The production of Ξ_{cc} through e^+e^- annihilation was investigated in previous studies [9, 10]. From figure 1 in ref. [10], it is evident that at $\sqrt{S} = 250\,\mathrm{GeV}$, the total cross section is approximately two orders of magnitude smaller than the presently predicted one via the LBS photoproduction and this difference shall become more pronounced as the collision energy increases. Therefore, the photoproduction process at higher collision energies on a high-luminosity e^+e^- collider offers a new potential venue for investigating the production of doubly charmed baryons. Conversely, we might also exploit this production channel to investigate the photoproduction mechanism.

Similarly, for the three collision energies, cross sections of various intermediate diquark states are provided in table 2. These results reveal that the contribution of S-wave diquarks is significantly larger than that of the P-wave diquarks. At $\sqrt{S} = 250\,\mathrm{GeV}$, the ratio between the contributions from the S-wave and P-wave is 18.7:1. At $\sqrt{S} = 500\,\mathrm{GeV}$, the ratio becomes 16.8:1, meaning that the P-wave contributions constitute 5.6% of the total production. Among the P-wave states, the contribution of the $(cc)_\mathbf{6}[^3P_2]$ diquark is the largest. Their ratio is as follows: $(cc)_{\bar{\mathbf{3}}}[^1P_1] : (cc)_\mathbf{6}[^3P_0] : (cc)_\mathbf{6}[^3P_1] : (cc)_\mathbf{6}[^3P_2]=1:0.23:0.32:1.52$ at $\sqrt{S} = 500\,\mathrm{GeV}$. Assuming an integrated luminosity of $\mathcal{O}(10^4)\,\mathrm{fb}^{-1}$ at future e^+e^- colliders and summing up the contributions from all P-wave excited baryons, approximately 2.9×10^5

$\sqrt{S}$(GeV)	$\gamma + \gamma \to \Xi_{cc} + \bar{c} + \bar{c}$	$\gamma + g \to \Xi_{cc} + \bar{c} + \bar{c}$	total
250	228.61(44.52)	238.90(15.79)	467.50(60.31)
500	101.34(65.25)	411.50(28.93)	512.84(94.19)
1000	40.94(97.82)	659.81(49.93)	700.75(147.76)

Table 1. The integrated cross sections (in unit of fb) from different channels for Ξ_{cc} photoproduction under various collision energies at future e^+e^- collider. The contributions from the S-wave and P-wave have been combined. The values in brackets are the cross sections via WWA photon.

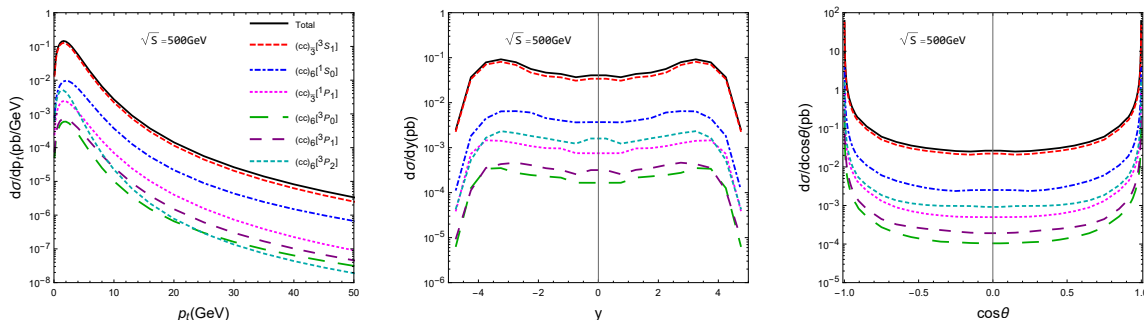| $\sqrt{S}$(GeV)	$(cc)_{\bar{\mathbf{3}}}[^3S_1]$	$(cc)_{\mathbf{6}}[^1S_0]$	$(cc)_{\bar{\mathbf{3}}}[^1P_1]$	$(cc)_{\mathbf{6}}[^3P_0]$	$(cc)_{\mathbf{6}}[^3P_1]$	$(cc)_{\mathbf{6}}[^3P_2]$
250	407.43	36.32	8.81	1.75	2.44	10.75
500	442.71	41.24	9.42	2.12	3.03	14.32
1000	603.0	57.05	12.66	2.97	4.33	20.72

Table 2. The integrated cross sections (in unit of fb) of different intermediate diquark states for Ξ_{cc} photoproduction under various collision energies at future e^+e^- collider.
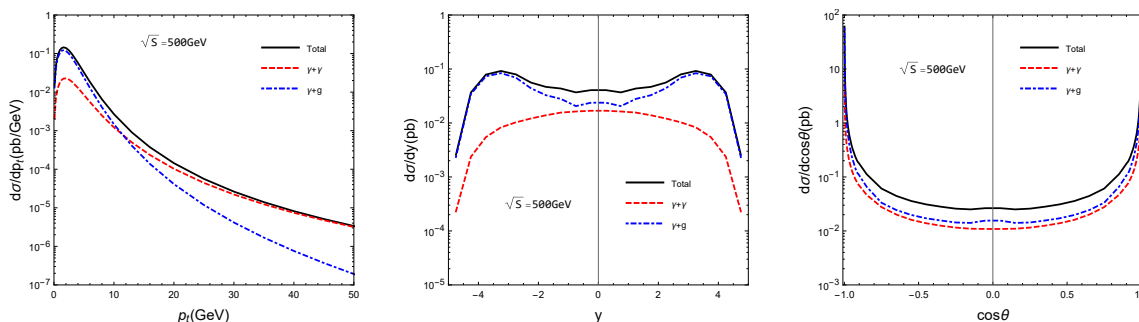
Figure 3. Kinematic distributions for the photoproduction of Ξ_{cc} at future e^+e^- collider($\sqrt{S}$ =500 GeV). Contributions from different channels are displayed individually.

P-wave Ξ_{cc} baryons would be generated, given a collision energy of $\sqrt{S} = 500$ GeV. The P-wave doubly charmed baryons are likely to decay to the ground state with almost 100% probability, making them additional sources of ground-state baryons.

To reveal more characteristics of Ξ_{cc} photoproduction at the e^+e^- collider, we have computed the differential distributions at $\sqrt{S} = 500\,\text{GeV}$, as illustrated in figure 3 and figure 4. Figure 3 depicts the transverse momentum(p_t), the rapidity(y) and $cos\theta$ distributions, featuring distinct representations of contributions originating from different channels. Here, θ represents the angle between Ξ_{cc} and the e^+e^- beams. The $\gamma + g$ channels exert their dominance in the lower p_t region, gradually passing the torch to the $\gamma + \gamma$ channels as the p_t values increase. In practical experiments, there may not be a sufficient number of events in the high p_t region to attain precise measurements. Consequently, it becomes necessary to consider the single resolved channel $\gamma + g$ when performing photoproduction calculations. In contrast to the curves for the p_t distribution, in the rapidity and angular distributions, the curves for the two production channels do not intersect. Throughout

Figure 4. Kinematic distributions for the photoproduction of Ξ_{cc} at future e^+e^- collider($\sqrt{S} =$500 GeV). Contributions from different diquark states are displayed individually. The y and $\cos\theta$ curves use same legends as those of p_t.

m_c(GeV)	$(cc)_{\bar{\mathbf{3}}}[^3S_1]$	$(cc)_{\mathbf{6}}[^1S_0]$	$(cc)_{\bar{\mathbf{3}}}[^1P_1]$	$(cc)_{\mathbf{6}}[^3P_0]$	$(cc)_{\mathbf{6}}[^3P_1]$	$(cc)_{\mathbf{6}}[^3P_2]$
1.7	609.62	56.85	14.50	3.28	4.67	22.27
1.8	442.71	41.24	9.42	2.12	3.03	14.32
1.9	328.38	30.53	6.24	1.40	2.0	9.45

Table 3. The total cross sections (in unit of fb) under different m_c at $\sqrt{S} = 500$ GeV.

$\mathcal{C}$	$(cc)_{\bar{\mathbf{3}}}[^3S_1]$	$(cc)_{\mathbf{6}}[^1S_0]$	$(cc)_{\bar{\mathbf{3}}}[^1P_1]$	$(cc)_{\mathbf{6}}[^3P_0]$	$(cc)_{\mathbf{6}}[^3P_1]$	$(cc)_{\mathbf{6}}[^3P_2]$
0.5	531.74	50.46	11.44	2.47	3.57	16.40
1.0	442.71	41.24	9.42	2.12	3.03	14.32
2.0	376.96	35.12	8.0	1.84	2.59	12.61

Table 4. The total cross sections (in unit of fb) under various $\mu(= \mathcal{C}\sqrt{M_{\Xi_{cc}}^2 + p_t^2}$ with $\mathcal{C} = 0.5, 1, 2)$ at $\sqrt{S} = 500$ GeV.

the entire rapidity distribution range, the contributions of $\gamma + g$ consistently surpass those of $\gamma + \gamma$. The same pattern is also evident in the angular distribution curves. Figure 4 displays the contribution curves for different intermediate diquark states. In each p_t distribution, a noticeable peak emerges at approximately several GeV, followed by a logarithmic decline in the high p_t region. In all three distinct kinematic distributions, it is consistently evident that the $_{\bar{\mathbf{3}}}[^3S_1]$ configurations maintain prominence across the entire range, while contributions from other states are small.

Finally, we delve into a brief discussion of the theoretical uncertainties inherent in our calculations, stemming from three main sources: the heavy quark mass m_c, the renormalization scale μ, and the LDMEs. It's worth noting that uncertainties originating from $h_{\bar{\mathbf{3}}}$ and $h_{\mathbf{6}}$ have been omitted due to the lack of reported errors in the literature. As mentioned earlier, these coefficients represent global factors, and their influence on production outcomes can be further refined with more precise values. Table 3 demonstrates the impact of changing the value of m_c within the range of 1.8 ± 0.1 GeV while keeping $\mu = \sqrt{M_{\Xi_{cc}}^2 + p_t^2}$

constant. As observed in the table, even small variations in the heavy quark mass can result in substantial fluctuations in cross-section values. For example, in table 3, the cross section for $(cc)_{\bar{\mathbf{3}}}[^3S_1]$ varies by approximately 46% with only a 12% change in m_c. This notable sensitivity becomes evident when analyzing the relevant Feynman diagrams, as exemplified in figure 2. For photoproduction of Ξ_{cc} considered here, it is noted that the final particles involved in the short-distance processes consist exclusively of c and $\bar{c}$, while the internal lines are composed solely of charm and gluon propagators. Therefore, the significant impact of heavy quark masses on the cross section appears to be a reasonable outcome. To illustrate the strong dependence on m_c, let's consider the first diagram in figure 2. The squared invariant mass of the gluon propagator attached to the final $c\bar{c}$ pair is given by $k^2 = (k_{12} + k_2)^2$. Its dominant region in phase space integration is near the threshold, i.e., when $k^2 \sim 4m_c^2$. As a result, when the value of m_c varies from $1.7\,\text{GeV}$ to $1.9\,\text{GeV}$, $1/(k^2)^2$ undergoes a approximately 36% change. It is worth noting that the charm mass also affects the cross section through the choice of the renormalization scale, which is set to $\mu = \sqrt{M_{\Xi_{cc}}^2 + p_t^2}$ in our calculations.

Table 4 evaluates the sensitivity to the renormalization scale ($\mu = \mathcal{C}\sqrt{M_{\Xi_{cc}}^2 + p_t^2}$, where $\mathcal{C} = 0.5, 1, 2$), while keeping the value of m_c fixed at 1.8 GeV. Clearly, there is a significant dependence on the renormalization scale, which could suggest the importance of next-to-leading order corrections in α_s. As we confront real-world measurements in the future, high-order calculations become imperative. Taking into account the aforementioned uncertainties, our leading-order calculation results may vary by approximately one order of magnitude. Despite this range of variability, the photoproduction rates of doubly charmed baryons remain significant.

4 Summary

In this work, we have investigated the Ξ_{cc} photoproduction within the framework of non-relativistic QCD specifically focusing on future e^+e^- colliders, where the initial photon beams are from laser-back scattering. Two dominant photoproduction processes are considered, i.e., $\gamma + \gamma \to \Xi_{cc} + \bar{c} + \bar{c}$ and $\gamma + g \to \Xi_{cc} + \bar{c} + \bar{c}$. Four P-wave diquark states are included in the calculation and they are $(cc)_{\bar{\mathbf{3}}}[^1P_1]$, $(cc)_{\mathbf{6}}[^3P_0]$, $(cc)_{\mathbf{6}}[^3P_1]$ and $(cc)_{\mathbf{6}}[^3P_2]$. Upon assuming $h_{\mathbf{6}} = h_{\bar{\mathbf{3}}}$, the results demonstrate the photoproduction of P-wave Ξ_{cc} is about one order lower than that of the S-wave. Specifically, at a center-of-mass energy of $\sqrt{S} = 500\,\text{GeV}$, the cross section for P-wave Ξ_{cc} production is approximately 6% of that for S-wave production. The numerical results further emphasize the crucial role played by the single resolved photoproduction channel $\gamma + g$ in the overall photoproduction process. It gains increasing significance as the collision energy rises. Assuming an integrated luminosity for future e^+e^- collisions on the order of $\mathcal{O}(10^4)\,\text{fb}^{-1}$, approximately 4.8×10^6 S-wave Ξ_{cc} and 2.9×10^5 P-wave Ξ_{cc} baryons would be expected to be produced at a collision energy of $\sqrt{S} = 500$ GeV. The excited doubly charmed baryons are likely to decay into the ground state with nearly 100% probability. Therefore, when faced with precise real-world measurements, their contributions should be thoroughly examined and taken into account.

Acknowledgments

References

[1] SELEX collaboration, *First observation of the doubly charmed baryon* Ξ_{cc}^+, *Phys. Rev. Lett.* **89** (2002) 112001 [`hep-ex/0208014`] [ɪɴSPIRE].

[2] SELEX collaboration, *Confirmation of the double charm baryon* $\Xi_{cc}^+(3520)$ *via its decay to* pD^+K^-, *Phys. Lett. B* **628** (2005) 18 [`hep-ex/0406033`] [ɪɴSPIRE].

[3] LHCb collaboration, *First observation of the doubly charmed baryon decay* $\Xi_{cc}^{++} \to \Xi_c^+\pi^+$, *Phys. Rev. Lett.* **121** (2018) 162002 [`arXiv:1807.01919`] [ɪɴSPIRE].

[4] LHCb collaboration, *Measurement of the lifetime of the doubly charmed baryon* Ξ_{cc}^{++}, *Phys. Rev. Lett.* **121** (2018) 052002 [`arXiv:1806.02744`] [ɪɴSPIRE].

[5] J.P. Ma and Z.G. Si, *Factorization approach for inclusive production of doubly heavy baryon*, *Phys. Lett. B* **568** (2003) 135 [`hep-ph/0305079`] [ɪɴSPIRE].

[6] G.T. Bodwin, E. Braaten and G.P. Lepage, *Rigorous QCD analysis of inclusive annihilation and production of heavy quarkonium*, *Phys. Rev. D* **51** (1995) 1125 [*Erratum ibid.* **55** (1997) 5853] [`hep-ph/9407339`] [ɪɴSPIRE].

[7] S.P. Baranov, *On the production of doubly flavored baryons in pp, ep and* $\gamma\gamma$ *collisions*, *Phys. Rev. D* **54** (1996) 3228 [ɪɴSPIRE].

[8] A.V. Berezhnoy, V.V. Kiselev and A.K. Likhoded, *Photonic production of S- and P-wave* B_c *states and doubly heavy baryons*, *Z. Phys. A* **356** (1996) 89 [ɪɴSPIRE].

[9] J. Jiang et al., *Doubly heavy baryon production at a high luminosity* e^+e^- *collider*, *Phys. Rev. D* **86** (2012) 054021 [`arXiv:1208.3051`] [ɪɴSPIRE].

[10] J. Jiang et al., *A further study on the doubly heavy baryon production around the* Z^0 *peak at a high luminosity* e^+e^- *collider*, *Phys. Rev. D* **87** (2013) 054027 [`arXiv:1302.0601`] [ɪɴSPIRE].

[11] G. Chen et al., *Photoproduction of doubly heavy baryon at the ILC*, *JHEP* **12** (2014) 018 [`arXiv:1408.4615`] [ɪɴSPIRE].

[12] Z.-J. Yang, P.-F. Zhang and Y.-J. Zheng, *Doubly heavy baryon production in* e^+e^- *annihilation*, *Chin. Phys. Lett.* **31** (2014) 051301 [ɪɴSPIRE].

[13] Z.-J. Yang and X.-X. Zhao, *The production of* Ξ_{bb} *at photon collider*, *Chin. Phys. Lett.* **31** (2014) 091301 [`arXiv:1408.5584`] [ɪɴSPIRE].

[14] X.-C. Zheng, C.-H. Chang and Z. Pan, *Production of doubly heavy-flavored hadrons at* e^+e^- *colliders*, *Phys. Rev. D* **93** (2016) 034019 [`arXiv:1510.06808`] [ɪɴSPIRE].

[15] H.-Y. Bi et al., *Photoproduction of doubly heavy baryon at the LHeC*, *Phys. Rev. D* **95** (2017) 074020 [arXiv:1702.07181] [InSPIRE].

[16] Z. Sun and X.-G. Wu, *The production of the doubly charmed baryon in deeply inelastic ep scattering at the Large Hadron electron Collider*, *JHEP* **07** (2020) 034 [arXiv:2004.01012] [InSPIRE].

[17] G. Chen et al., *Hadronic production of Ξ_{cc} at a fixed-target experiment at the LHC*, *Phys. Rev. D* **89** (2014) 074020 [arXiv:1401.6269] [InSPIRE].

[18] G. Chen, X.-G. Wu and S. Xu, *Impacts of the intrinsic charm content of the proton on the Ξ_{cc} hadroproduction at a fixed target experiment at the LHC*, *Phys. Rev. D* **100** (2019) 054022 [arXiv:1903.00722] [InSPIRE].

[19] G. Chen, C.-H. Chang and X.-G. Wu, *Hadronic production of the doubly charmed baryon via the proton-nucleus and the nucleus-nucleus collisions at the RHIC and LHC*, *Eur. Phys. J. C* **78** (2018) 801 [arXiv:1808.03174] [InSPIRE].

[20] A.P. Martynenko and A.M. Trunin, *Pair double heavy diquark production in high energy proton-proton collisions*, *Eur. Phys. J. C* **75** (2015) 138 [arXiv:1405.0969] [InSPIRE].

[21] S. Koshkarev, *Production of the doubly heavy baryons, B_c meson and the all-charm tetraquark at AFTER@LHC with double intrinsic heavy mechanism*, *Acta Phys. Polon. B* **48** (2017) 163 [arXiv:1610.06125] [InSPIRE].

[22] S. Koshkarev and V. Anikeev, *Production of the doubly charmed baryons at the SELEX experiment — the double intrinsic charm approach*, *Phys. Lett. B* **765** (2017) 171 [arXiv:1605.03070] [InSPIRE].

[23] S. Groote and S. Koshkarev, *Production of doubly charmed baryons nearly at rest*, *Eur. Phys. J. C* **77** (2017) 509 [arXiv:1704.02850] [InSPIRE].

[24] A.V. Berezhnoy, A.K. Likhoded and A.V. Luchinsky, *Doubly heavy baryons at the LHC*, *Phys. Rev. D* **98** (2018) 113004 [arXiv:1809.10058] [InSPIRE].

[25] S.J. Brodsky, S. Groote and S. Koshkarev, *Resolving the SELEX-LHCb double-charm baryon conflict: the impact of intrinsic heavy-quark hadroproduction and supersymmetric light-front holographic QCD*, *Eur. Phys. J. C* **78** (2018) 483 [arXiv:1709.09903] [InSPIRE].

[26] A.V. Berezhnoy, I.N. Belov and A.K. Likhoded, *Production of doubly charmed baryons with the excited heavy diquark at LHC*, *Int. J. Mod. Phys. A* **34** (2019) 1950038 [arXiv:1811.07382] [InSPIRE].

[27] X.-G. Wu, *A new search for the doubly charmed baryon Ξ_{cc}^+ at the LHC*, *Sci. China Phys. Mech. Astron.* **63** (2020) 221063 [arXiv:1912.01953] [InSPIRE].

[28] Q. Qin, Y.-F. Shen and F.-S. Yu, *Discovery potentials of double-charm tetraquarks*, *Chin. Phys. C* **45** (2021) 103106 [arXiv:2008.08026] [InSPIRE].

[29] J.-J. Niu et al., *Production of semi-inclusive doubly heavy baryons via top-quark decays*, *Phys. Rev. D* **98** (2018) 094021 [arXiv:1810.03834] [InSPIRE].

[30] J.-J. Niu, L. Guo, H.-H. Ma and X.-G. Wu, *Production of doubly heavy baryons via Higgs boson decays*, *Eur. Phys. J. C* **79** (2019) 339 [arXiv:1904.02339] [InSPIRE].

[31] P.-H. Zhang, L. Guo, X.-C. Zheng and Q.-W. Ke, *Excited doubly heavy baryon production via W^+ boson decays*, *Phys. Rev. D* **105** (2022) 034016 [arXiv:2202.01579] [InSPIRE].

[32] H.-H. Ma and J.-J. Niu, *Excited doubly heavy baryons production via Higgs decays*, *Eur. Phys. J. C* **83** (2023) 5 [arXiv:2212.12626] [INSPIRE].

[33] X. Luo, Y.-Z. Jiang, G.-Y. Zhang and Z. Sun, *Doubly-charmed baryon production in Z boson decay*, arXiv:2206.05965 [INSPIRE].

[34] X. Luo, H.-B. Fu and H.-J. Tian, *Investigation of Z-boson decay into and baryons within the NRQCD factorization approach**, *Chin. Phys. C* **47** (2023) 053102 [arXiv:2208.07520] [INSPIRE].

[35] H.-H. Ma, J.-J. Niu and X.-C. Zheng, *Excited doubly heavy baryons production via top-quark decays*, *Phys. Rev. D* **107** (2023) 014006 [arXiv:2210.03306] [INSPIRE].

[36] J.-J. Niu, J.-B. Li, H.-Y. Bi and H.-H. Ma, *Production of excited doubly heavy baryons at the super-Z factory*, *Eur. Phys. J. C* **83** (2023) 822 [arXiv:2305.15362] [INSPIRE].

[37] H.-J. Tian, X. Luo and H.-B. Fu, *Further study on the production of P-wave doubly heavy baryons from Z-boson decays*, arXiv:2306.03388 [INSPIRE].

[38] C.-H. Chang, J.-X. Wang and X.-G. Wu, *GENXICC: a generator for hadronic production of the double heavy baryons Ξ_{cc}, Ξ_{bc} and Ξ_{bb}*, *Comput. Phys. Commun.* **177** (2007) 467 [hep-ph/0702054] [INSPIRE].

[39] C.-H. Chang, J.-X. Wang and X.-G. Wu, *GENXICC2.0: an upgraded version of the generator for hadronic production of double heavy baryons Ξ_{cc}, Ξ_{bc} and Ξ_{bb}*, *Comput. Phys. Commun.* **181** (2010) 1144 [arXiv:0910.4462] [INSPIRE].

[40] X.-Y. Wang and X.-G. Wu, *GENXICC2.1: an improved version of GENXICC for hadronic production of doubly heavy baryons*, *Comput. Phys. Commun.* **184** (2013) 1070 [arXiv:1210.3458] [INSPIRE].

[41] FCC collaboration, *FCC-ee: the lepton collider. Future Circular Collider conceptual design report volume 2*, *Eur. Phys. J. ST* **228** (2019) 261 [INSPIRE].

[42] CEPC STUDY GROUP collaboration, *CEPC conceptual design report: volume 1 — accelerator*, arXiv:1809.00285 [INSPIRE].

[43] CEPC STUDY GROUP collaboration, *CEPC conceptual design report: volume 2 — physics & detector*, arXiv:1811.10545 [INSPIRE].

[44] ILC collaboration, *International Linear Collider reference design report volume 2: physics at the ILC*, arXiv:0709.1893 [INSPIRE].

[45] J. Erler et al., *Physics impact of GigaZ*, *Phys. Lett. B* **486** (2000) 125 [hep-ph/0005024] [INSPIRE].

[46] M. Klasen, B.A. Kniehl, L.N. Mihaila and M. Steinhauser, *Evidence for color octet mechanism from CERN LEP-2 $\gamma\gamma \to J/\psi + X$ data*, *Phys. Rev. Lett.* **89** (2002) 032001 [hep-ph/0112259] [INSPIRE].

[47] R. Li and K.-T. Chao, *Photoproduction of J/psi in association with a $c\bar{c}$ pair*, *Phys. Rev. D* **79** (2009) 114020 [arXiv:0904.1643] [INSPIRE].

[48] X.-J. Zhan and J.-X. Wang, *Prompt J/ψ photoproduction within the non-relativistic QCD framework at the CEPC*, *Eur. Phys. J. C* **80** (2020) 740 [arXiv:2005.08816] [INSPIRE].

[49] X.-J. Zhan and J.-X. Wang, *Inclusive $\Upsilon(1S, 2S, 3S)$ photoproduction at the CEPC*, *Chin. Phys. C* **45** (2021) 023112 [INSPIRE].

[50] X.-J. Zhan, X.-G. Wu and X.-C. Zheng, *Inclusive J/ψ photoproduction at the ILC within the framework of non-relativistic QCD*, *JHEP* **09** (2022) 050 [`arXiv:2207.01763`] [ɪɴSPIRE].

[51] X.-J. Zhan, X.-G. Wu and X.-C. Zheng, *Photoproduction of the B_c meson at future e^+e^- colliders*, *Phys. Rev. D* **106** (2022) 094036 [`arXiv:2211.09003`] [ɪɴSPIRE].

[52] S. Frixione, M.L. Mangano, P. Nason and G. Ridolfi, *Improving the Weizsacker-Williams approximation in electron-proton collisions*, *Phys. Lett. B* **319** (1993) 339 [`hep-ph/9310350`] [ɪɴSPIRE].

[53] I.F. Ginzburg, G.L. Kotkin, V.G. Serbo and V.I. Telnov, *Colliding γe and γγ beams based on the single pass accelerators (of VLEPP type)*, *Nucl. Instrum. Meth.* **205** (1983) 47 [ɪɴSPIRE].

[54] V.I. Telnov, *Problems of obtaining γγ and γϵ colliding beams at linear colliders*, *Nucl. Instrum. Meth. A* **294** (1990) 72 [ɪɴSPIRE].

[55] G.C. Nayak, J.-W. Qiu and G.F. Sterman, *Fragmentation, factorization and infrared poles in heavy quarkonium production*, *Phys. Lett. B* **613** (2005) 45 [`hep-ph/0501235`] [ɪɴSPIRE].

[56] G.C. Nayak, J.-W. Qiu and G.F. Sterman, *Fragmentation, NRQCD and NNLO factorization analysis in heavy quarkonium production*, *Phys. Rev. D* **72** (2005) 114012 [`hep-ph/0509021`] [ɪɴSPIRE].

[57] G.C. Nayak, J.-W. Qiu and G.F. Sterman, *NRQCD factorization and velocity-dependence of NNLO poles in heavy quarkonium production*, *Phys. Rev. D* **74** (2006) 074007 [`hep-ph/0608066`] [ɪɴSPIRE].

[58] M. Gluck, E. Reya and I. Schienbein, *Radiatively generated parton distributions of real and virtual photons*, *Phys. Rev. D* **60** (1999) 054019 [*Erratum ibid.* **62** (2000) 019902] [`hep-ph/9903337`] [ɪɴSPIRE].

[59] A.F. Falk, M.E. Luke, M.J. Savage and M.B. Wise, *Heavy quark fragmentation to baryons containing two heavy quarks*, *Phys. Rev. D* **49** (1994) 555 [`hep-ph/9305315`] [ɪɴSPIRE].

[60] V.V. Kiselev, A.K. Likhoded and M.V. Shevlyagin, *Double charmed baryon production at B factory*, *Phys. Lett. B* **332** (1994) 411 [`hep-ph/9408407`] [ɪɴSPIRE].

[61] E. Bagan et al., *Hadrons with charm and beauty*, *Z. Phys. C* **64** (1994) 57 [`hep-ph/9403208`] [ɪɴSPIRE].

[62] A.V. Berezhnoy, V.V. Kiselev, A.K. Likhoded and A.I. Onishchenko, *Doubly charmed baryon production in hadronic experiments*, *Phys. Rev. D* **57** (1998) 4385 [`hep-ph/9710339`] [ɪɴSPIRE].

[63] D. Binosi and L. Theussl, *JaxoDraw: a graphical user interface for drawing Feynman diagrams*, *Comput. Phys. Commun.* **161** (2004) 76 [`hep-ph/0309015`] [ɪɴSPIRE].

[64] V.V. Kiselev, A.K. Likhoded, O.N. Pakhomova and V.A. Saleev, *Mass spectra of doubly heavy $\Omega_{QQ'}$ baryons*, *Phys. Rev. D* **66** (2002) 034030 [`hep-ph/0206140`] [ɪɴSPIRE].